LETTER

# 587 nm nanosecond optical pulse generation by synchronously-driven gain-switched laser diodes with optical injection locking

Applied Physics Express 12, 082002 (2019)
https://doi.org/10.7567/1882-0786/ab2c2a

LETTER

# 587 nm nanosecond optical pulse generation by synchronously-driven gain-switched laser diodes with optical injection locking

Jui-Hung Hung[1], Yuan Gao[2], Hejie Yan[2], Kazuo Sato[1], Hirohito Yamada[1,2], Lung-Han Peng[1,3], Tomomi Nemoto[4,5], and Hiroyuki Yokoyama[1,2*]

[1]New Industry Creation Hatchery Center, Tohoku University, Sendai, 980-8579, Japan
[2]Graduate School of Engineering, Tohoku University, Sendai, 980-8579, Japan
[3]Graduate Institute of Photonics and Optoelectronics, National Taiwan University, Taipei 10617, Taiwan, Republic of China
[4]Research Institute for Electronic Science, Hokkaido University, Sapporo 001-0020, Japan
[5]Graduate School of Information Science and Technology, Hokkaido University, Sapporo 060-0814, Japan

*E-mail: yoko@niche.tohoku.ac.jp

Received April 23, 2019; revised June 20, 2019; accepted June 24, 2019; published online July 9, 2019

We describe a novel optical pulse source that can generate yellow-orange optical pulses based on the synchronization of two gain-switched laser diodes under continuous-wave laser light injection. Sum frequency generation of amplified 1309 nm and 1064 nm optical pulses produced 587 nm pulses with 1 ns duration and 2 nJ pulse energy at a repetition rate of 5 MHz. The presented optical pulse source can also produce bursts of picosecond optical pulses inside nanosecond pulse envelopes. These optical pulses are applicable to stimulated emission depletion microscopy for super-resolution imaging of biomedical specimens with green- or yellow- fluorescent proteins labels.


Stimulated emission depletion (STED) microscopy has been widely used to envision biomedical specimens to a sub-diffraction-limit resolution.[1,2] In general, a continuous-wave (CW) laser source with an average power at the Watt-level is required for STED microscopy. This high average power usually causes photobleaching of fluorescent labels and this impairs the reliability for in vivo imaging.[3] The average power of a STED beam can be reduced to the milliwatt-level by using a pulsed-STED beam with a pulse duration of 0.1–1 ns and a pulse energy at nano-joule level.[4] Despite the advantages of pulsed sources, many biologists resorted to CW-STED implementation in the last decade because of the limited availability of practical optical pulse sources that can satisfy the demands of STED microscopy.

We previously demonstrated an optical pulse source that was capable of generating sub-nanosecond, 650 nm optical pulses that satisfied the requirements for STED.[5] In that case, the core technology was the gain-switching operation of a semiconductor-laser optical amplifier (GS-SOA) for generating smooth-shaped single-peak, sub-nanosecond optical pulses at 1.3 $\mu$m. The optical pulses generated were then amplified using an optical fiber amplifier (OFA) and subsequently converted to second harmonic (SH) light using a nonlinear-optic crystal. This 650 nm optical pulse source proved to be beneficial for sub-100 nm resolution STED imaging[6] of bio-specimens labeled with red-color fluorescent molecules owing to an enhancement of the optical pulse energy of more than an order of magnitude, compared to the case of a visible-laser diode (LD).[7]

Currently, the most commonly used fluorescent labels are green-fluorescent-protein (GFP) and yellow-fluorescent-protein (YFP). An optical pulse source with an emission wavelength of 570–610 nm is required for STED imaging when these fluorescent proteins are utilized. However, there are few optical pulse sources suitable for STED microscopy in this wavelength region. Conventionally, the combination of a mode-locked Ti:Sapphire laser and a nonlinear-optic parametric oscillator has been successfully applied for STED, but the overall laser system is complex and large-sized.[2] Recently, several approaches based on stimulated Raman scattering (SRS) in optical fibers have been reported.[8–10] Although optical pulses with a nanosecond duration and sufficient pulse energy can be provided, accurate control of the optical pulse shape and the duration is difficult. Moreover, stabilizing the power of the wavelength-converted output is challenging owing to the existence of higher order SRS processes.

In this report, we describe a new approach to realize an optical pulse source designed for pulsed-mode STED microscopy of bio-specimens expressing GFP or YFP. This optical pulse source enables long-term stable operation based on semiconductor-laser controlling technologies, and can generate 587 nm optical pulses with nano-joule pulse energy at a multi-megahertz repetition rate based on the sum-frequency-generation (SFG) of synchronized 1.3 $\mu$m and 1.06 $\mu$m nanosecond optical pulses generated from LDs. Another notable feature is that the present optical pulse source configuration can also generate bursts of picosecond optical pulses within nanosecond pulse envelopes. This operation mode can potentially facilitate superior nonlinear-optic wavelength conversion efficiency as will be described subsequently. Moreover, the entire pulse envelope duration is equivalent to that of a single nanosecond optical pulse duration from the perspective of STED application.

Our concept is to produce optical pulses from synchronously-driven 1.3 $\mu$m and 1.06 $\mu$m gain-switched LDs (GS-LDs). Thereafter, these optical pulses are amplified using appropriate OFAs and subsequently converted to 587 nm via an SFG process using a nonlinear-optic crystal. A schematic of the 587 nm optical pulse source is shown in Fig. 1. The entire configuration is indicated in Fig. 1(a), while a more detailed configuration for an optical pulse generator is schematically shown in Fig. 1(b).

To perform visible optical pulse generation via SFG, in addition to the synchronization of 1.3 $\mu$m and 1.06 $\mu$m optical pulses, narrow line-width laser oscillations at both wavelengths are essential to satisfy the requirement of narrow-bandwidth phase matching condition. Therefore, we introduced a CW single-mode laser light injection for two different Fabry–Perot LDs (FP-LDs) under gain-switching

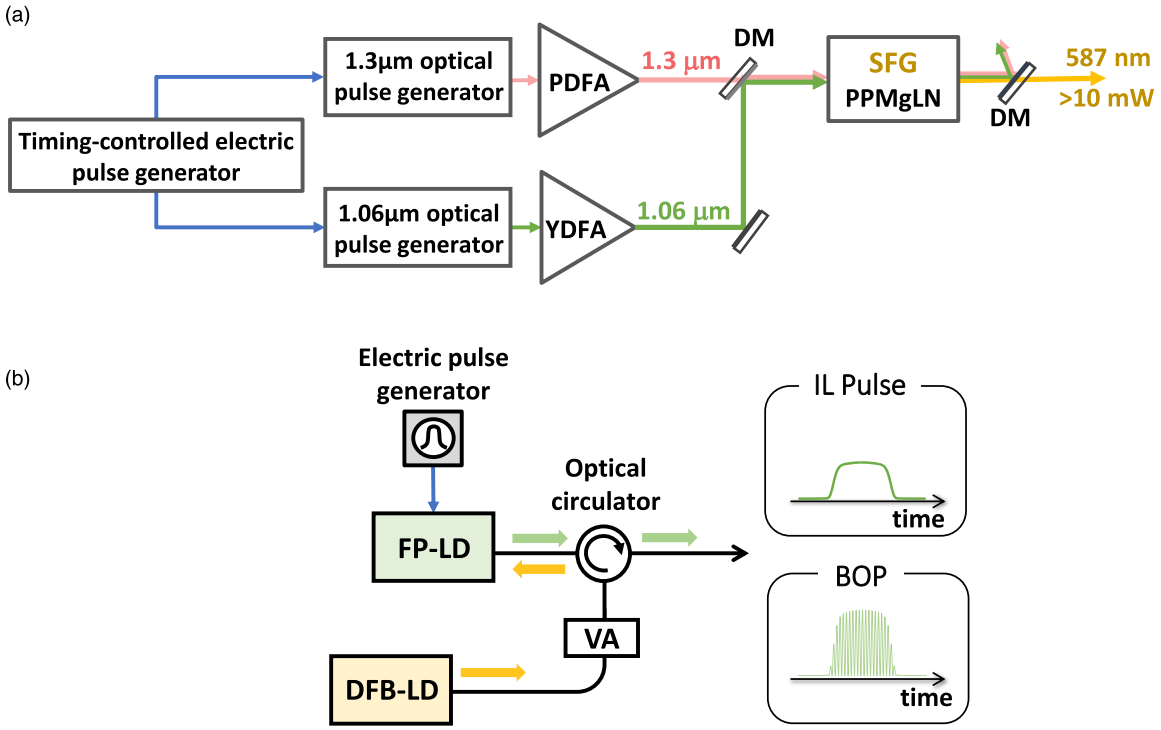


**Fig. 1.** (Color online) (a) Schematic configuration of 587 nm optical pulse generation via SFG of 1.3 $\mu$m and 1.06 $\mu$m optical pulses. PDFA: Pr-doped fiber amplifier; DM: dichroic mirror; YDFA: Yb-doped fiber amplifier; PPMgLN: magnesium-oxide doped periodically-poled lithium niobate. (b) The detailed configuration for each optical pulse generator shown in (a). FP-LD: Fabry–Perot laser diode, DFB-LD: distributed-feedback laser diode, VA: variable optical attenuator.

(GS) operation. A distributed-feedback LD (DFB-LD) was utilized as the single-mode laser light source for each wavelength region. Based on computer simulation analyses that were performed in advance of the experimental study, it was expected that an injection locking (IL) scheme could eliminate the relaxation oscillation features of a GS-LD, and thus produce smooth-shaped nanosecond (or sub-nanosecond) optical pulses. Furthermore, we found that controlling the duration and the shape of optical pulses is even more flexible for an injection-locked and gain-switched LD (ILGS-LD) in comparison with the GS-SOA scheme that was previously used.[5)]

It should be noted that the present ILGS-LD configuration can produce not only smooth-shaped nanosecond optical pulses but also bursts of picosecond optical pulses inside a single nanosecond pulse envelope by appropriately adjusting the operating conditions from that for complete IL pulse operation.[11)] In principle, this optical pulse feature (it is described as burst-optical-pulse: BOP) facilitates the enhancement of the SFG conversion efficiency owing to an increase in the optical pulse peak power.

In the actual experimental setup, a 1.3 $\mu$m optical pulse generator was constructed using an FP-LD module (Anritsu, GF3B5004DLW), and a DFB-LD module (Optilab, DFB-PM-1310 nm) and optically connected via a variable optical attenuator (Thorlabs, VOA50PM-APC) and an optical circulator (Lightstar Technology, PMOC-1310-3-A-F-0-2-1-2). For the 1.06 $\mu$m optical pulse generator, the devices used were as follows: FP-LD (LD-PD Inc., PL-FP-1064-B-1-PA-14BF), DFB-LD (QD Laser Co., QLD1061), variable optical attenuator (Thorlabs, VOA1064PM-APC), and an optical circulator (AFR, PMCIR-06-1-2-L-Q). All the connection fibers were polarization-maintained types. The 1.3 $\mu$m and 1.06 $\mu$m FP-LDs were synchronously driven by a multi-channel electric pulse generator (Stanford Research System, DG645). We set the pulse repetition to 5 MHz considering the image-data acquisition speed in actual STED imaging applications. The generated 1.3 $\mu$m optical pulses were amplified using a two-stage Praseodymium-doped fiber amplifier (PDFA: Fiberlabs Inc., AMP-FL8611-OB), while the generated 1.06 $\mu$m optical pulses were amplified using a three-stage homemade Ytterbium-doped fiber amplifier (YDFA). These two kinds of amplified optical pulses were free-space coupled using collimators lenses ($f = 4$ mm for 1.3 $\mu$m, and $f = 2.5$ mm for 1.06 $\mu$m) and combined using a dichroic mirror. The collinear beams were subsequently focused by a focusing lens ($f = 15$ mm) into a 10 mm long periodic-poled magnesium-oxide doped lithium niobate (PPMgLN) crystal (fabricated by HC Photonics Corp.) to generate SFG pulses. In our design, it was estimated that the two-wavelength laser beams would be focused at the center of the PPMgLN crystal with a beam-waist of 38 $\mu$m and a confocal parameter of 3.6 mm for the 1.3 $\mu$m light, and a beam-waist of 40 $\mu$m and a 5 mm confocal parameter for the 1.06 $\mu$m light. The crystal used had a 9.42 $\mu$m poling period and was operated at a temperature of 45 °C to satisfy the SFG phase matching condition. Both the crystal facets were antireflection coated ($R < 0.5\%$ for 1.3 $\mu$m, 1.06 $\mu$m and 587 nm bands). Another dichroic mirror was positioned after the SFG crystal to remove the residual 1.3 $\mu$m and 1.06 $\mu$m optical pulse beams.

Figure 2 indicates some representative temporal and spectral data for the 1.3 $\mu$m GS-LD optical pulses; Figs. 2(a) and 2(b) are for the cases without CW laser light injection, Figs. 2(c) and 2(d) are for a complete ILGS operation, Figs. 2(e) and 2(f) are for BOP mode. Temporal

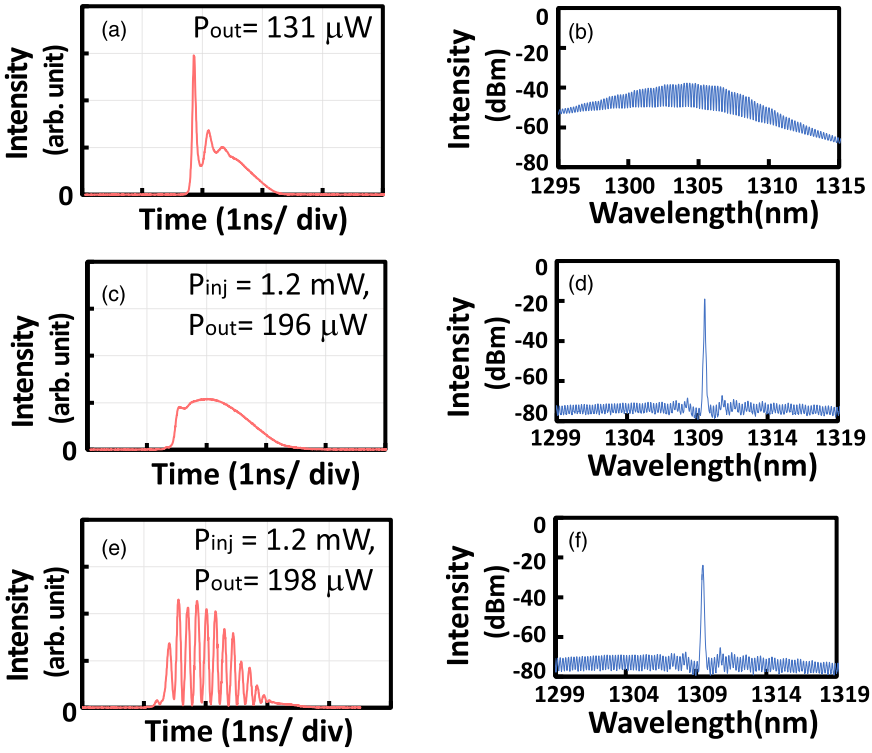


**Fig. 2.** (Color online) Oscilloscope temporal traces (a), (c), (e) and optical spectra (b), (d), (f) for 1.3 $\mu$m GS-LD optical pulses. (a), (b) are the cases without CW laser light injection, (c), (d) are for complete injection-locked operation, and (e), (f) are for BOP mode operation. $P_{inj}$ denotes the CW injection laser light power, and $P_{out}$ denotes the averaged optical pulse output power. See the text for detailed explanations of the figures and the device operating conditions.

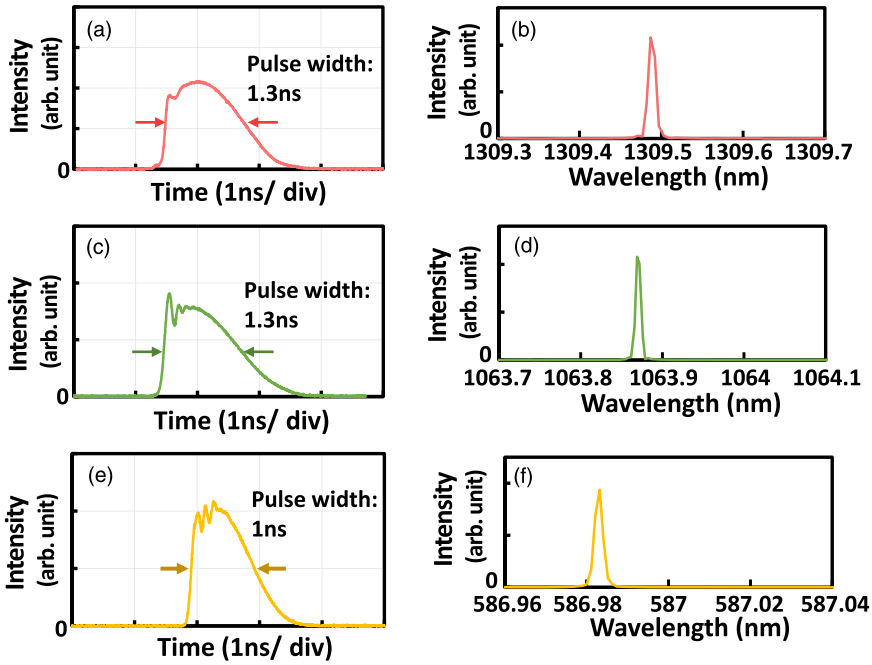


**Fig. 3.** (Color online) Oscilloscope temporal traces (a), (c), (e) and optical spectra (b), (d), (f) for 1.3 $\mu$m, 1.06 $\mu$m, and 587 nm optical pulses for the case of complete injection-locked operation for both 1.3 $\mu$m FP-LD, and 1.06 $\mu$m FP-LD. See text for detailed operating conditions of the devices.

traces for the optical pulses were recorded using the combination of an InGaAs photo-detector (PD) (New Focus, 1414, 25-GHz bandwidth) and a sampling oscilloscope (Agilent, 86100C, 40-GHz bandwidth) with sixteen times waveform averaging. In the case of this measurement, the excitation electric pulse conditions were set as amplitude: 4.7 V, repetition rate: 5 MHz, pulse duration: 4.1 ns. In Fig. 2(a), a typical initial relaxation oscillation pulse feature was observed, and the spectrum in Fig. 2(b) shows a multi-longitudinal-mode oscillation for GS operation of an FP-LD. In contrast, the temporal and spectral features significantly changed when a complete IL operation occurred, as shown in Figs. 2(c) and 2(d). The oscillation wavelength was exactly locked to the injection laser light wavelength (1309.5 nm), and the 1.3 ns temporal waveform duration does not involve sharp relaxation oscillation pulses. For the experimental

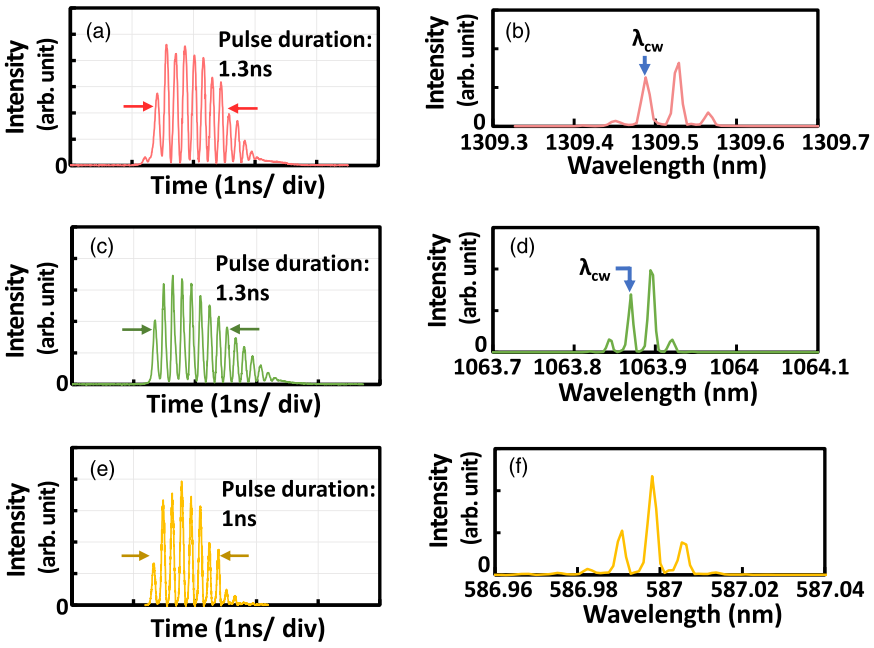


**Fig. 4.** (Color online) Oscilloscope temporal traces (a), (c), (e) and optical spectra (b), (d), (f) for 1.3 $\mu$m, 1.06 $\mu$m, and 587 nm optical pulses for the case of BOP mode operation for both 1.3 $\mu$m FP-LD, and 1.06 $\mu$m FP-LD. See text for detailed explanations of the figures and the device operating conditions.

results shown in Figs. 2(c) and 2(d), the DFB-LD temperature was set to 24.8 °C, the FP-LD temperature was 21 °C, and the CW laser light power injected into the FP-LD was set to 1.2 mW. It should be noted that the LD temperatures were stabilized within an accuracy of 0.1 °C, and stable IL operation was confirmed for several tens of hour (measurement time limit). The averaged optical output power from the circulator was ~0.19 mW under ILGS operation, while in the case without electric pulse excitation, the output was one order of magnitude lower. By changing the FP-LD temperature to 22 °C, BOP mode operation was initiated instead of the complete ILGS; Figs. 2(e) and 2(f) represent the temporal and the spectral data for this situation. In the temporal trace of Fig. 2(e), 70 ps duration short pulses with 160-ps pulse interval are involved in 1.3 ns envelope. It should be noted that the optical pulse peak power is two times higher compared to the ILGS optical pulses shown in Fig. 2(c). Although the spectral data of Fig. 2(f) seems to be similar to that of Fig. 2(d), it contains multi-spectral components as described later (Fig. 4).

To generate 587 nm SFG pulses, we first employed smooth-shaped ILGS-LD optical pulses for both the 1.3 $\mu$m and 1.06 $\mu$m fundamental wavelengths. Figures 3(a) and 3(b) show the temporal and spectral data for the 1.3 $\mu$m optical pulses after amplification by the PDFA to an average power of 74 mW. No temporal distortion was found after the amplification. The spectrum measured by an interferometer-type OSA (Advantest, Q8347) indicates the resolution limit width (0.005 nm for 1.3 $\mu$m band). Similar features were found for the 1.06 $\mu$m band ILGS optical pulses as shown in Figs. 3(c) and 3(d). The electric pulse excitation conditions for the 1.06 $\mu$m FP-LD were: 3.8 V amplitude, 2.1 ns pulse duration, and the injection CW laser light power was 2.2 mW at 1063.9 nm. The temperatures of the LDs were set to be 22 °C for the FP-LD and 21.5 °C for the DFB-LD. The resulting 1.06 $\mu$m optical pulses had a duration of 1.3 ns (FWHM) and an averaged output power of 67 $\mu$W. After amplification by the YDFA, the maximum average power of the 1.06 $\mu$m optical pulses increased to 190 mW. A temporal waveform obtained from an oscilloscope and a spectrum of an SFG-converted optical pulse are shown in Figs. 3(e) and 3(f), respectively. The spectral width of the 587 nm pulses was also at the resolution limit of the OSA (0.001 nm at 587 nm band). The peak wavelength position of the SFG optical pulse is 586.98 nm, which is exactly coincident with the value calculated for the two wavelengths of the fundamental optical pulse. The maximal averaged SFG power was approximately 10 mW, which indicates an SFG conversion efficiency of 13.5% based on the averaged output power of 74 mW for the 1.3 $\mu$m optical pulses (taking the 1.06 $\mu$m optical pulse power to be the pump because of its higher average power). The 587 nm optical pulses had 2 nJ pulse energy and 1 ns pulse duration (FWHM), which corresponds to a peak power of 2 W. Based on previously reported results,[12,13] this pulse energy is quite sufficient to induce STED effects for bio-specimens expressing GFP and YFP. However, if a higher average power and a higher pulse energy are required for the 587 nm optical pulses, these can be increased by increasing the output power capacity in 1.3 $\mu$m and/or 1.06 $\mu$m optical fiber amplifiers.

We also attempted SFG via the synchronization of BOPs from 1.3 $\mu$m and 1.06 $\mu$m LDs. The optical pulse period inside a BOP pulse envelope is controllable via the operating conditions of the FP-LD and the power of the CW injection laser light. An advantage of synchronized BOPs for SFG is the higher peak power of the optical pulses in comparison to the case of ILGS-LD optical pulses with the same pulse envelope duration and the same averaged optical power. If the peak power is two-time higher, the expected SFG conversion efficiency can also be doubled for ideally synchronized two-wavelength BOPs. Because clear BOP oscilloscope traces were observed as shown in Fig. 2(e), no intentional stabilization was adopted for the internal optical pulse period in the present experiment. The operating

conditions for generating 1.3 $\mu$m BOPs were the same as that described in Fig. 2(e). However, to obtain more precise LD temperature control at 1.06 $\mu$m, we replaced the 1.06 $\mu$m FP-LD (Qphotonics, QFLD-1060-50S-BTF) and stabilized its operation at 24.5 °C and controlled the 1.06 $\mu$m CW injection laser power to 0.6 mW. Figure 4(a) shows a temporal trace for the 1.3 $\mu$m BOPs after amplification by the PDFA to 74 mW; this value is the same as that of the complete ILGS optical pulses shown in Fig. 3(a). The optical spectrum shown in Fig. 4(b) clearly shows two major peaks separated by 0.036 nm; the shorter wavelength peak represents the injection laser light while the other corresponds to the FP-LD oscillation mode, shifted by the laser light injection. The 0.036 nm wavelength separation corresponds to 6.3 GHz in the frequency domain, and this is coincident with the repetition rate of optical pulses inside the BOP envelope. The main mechanism for BOP generation is considered, in brief, to be the beating between the injection laser light and the dominant FP laser oscillation mode component outlived under the CW laser light injection during GS operation. It is also noted in Fig. 4(b) that four-wave mixing (FWM) of the two major spectral components clearly occurred beside both major peaks. Although similar types of FWM phenomena have been investigated to date,[14,15] the FWM conversion efficiency in the present experiment is more than 10% and this relatively strong FWM is probably due to the high-intensity laser light in the FP-LD under GS operation. Similar operation features were observed for the 1.06 $\mu$m BOPs by setting the appropriate driving conditions and the 1.06 $\mu$m BOPs were amplified to 190 mW by the YDFA; Figs. 4(c) and 4(d) represent a temporal trace and an optical spectrum for the BOPs, respectively. In practice, the 1.3 $\mu$m and 1.06 $\mu$m BOPs were carefully controlled to maximize the SFG power. The 587 nm SFG optical output then exhibited similar BOP features as shown in Figs. 4(e) and 4(f) with a maximal SFG power of 13 mW. This SFG power is 30% higher compared to the complete ILGS-LD pulses, but lower than the expected value of twofold. The main reason for this discrepancy seems to be a relative timing fluctuation between the two-wavelength BOPs. An rms relative timing-jitter of 30 ps was evaluated from oscilloscope measurement, and this value is closed to half the duration of the optical pulse inside the BOP. Nevertheless, this problem can be solved by further stabilization of the BOPs, for example, using a high precision electric pulse generator.

Based on a rate equation analysis, we found that BOPs can provide a fluorescent depletion efficiency equivalent to that with smooth-shaped pulses when two different kinds of optical pulses have the same pulse energy and same pulse envelope duration. However, in actuality, the SFG efficiency via second-order nonlinear-optic wavelength conversion process is better for the BOP case because of its higher peak power feature as shown in the previous sections. Therefore, the 587 nm BOPs can be beneficial for enhancing the STED effect due to their better power budget in comparison with the case for the smooth-shaped ILGS optical pulses.

In summary, we have described a new approach for the generation of yellow-orange nanosecond optical pulses towards application for pulsed-STED microscopy. Based on optically injection-locked GS-LD technology, duration-tunable smooth-shaped optical pulses were synchronously generated from 1.3 $\mu$m and 1.06 $\mu$m LDs, and SFG of the amplified 1.3 $\mu$m and 1.06 $\mu$m optical pulses produced 587 nm optical pulses with 2 nJ pulse energy at a repetition rate of 5 MHz. Furthermore, we also demonstrated that precise control of the GS-LD can generate BOPs with a higher peak power compared to completely injection-locked GS-LD optical pulses, which results in a higher SFG conversion efficiency. The approach described herein will be beneficial to STED super-resolution microscopy of bio-specimens expressing GFP and YFP in combination with GS-LD-based picosecond optical pulse sources for excitation.[6,7,16]

**Acknowledgments** This work was supported, in part, by "Brain Mapping by Integrated Neurotechnologies for Disease Studies (Brain/MINDS)" from Japan Agency for Medical Research and Development (AMED).

1) S. W. Hell, Science **316**, 1153 (2007).
2) P. Bianchini, C. Peres, M. Oneto, S. Galiani, G. Vicidomini, and A. Diaspro, Cell and Tissue Research **360**, 143 (2015).
3) M. Bouzin, G. Chirico, L. D'Alfonso, L. Sironi, G. Soavi, G. Cerullo, B. Campanini, and M. Collini, J. Phys. Chem. B **117**, 16405 (2013).
4) K. I. Willig, B. Harke, R. Medda, and S. W. Hell, Nat. Methods **4**, 915 (2007).
5) J.-H. Hung, K. Sato, Y.-C. Fang, L.-H. Peng, T. Nemoto, and H. Yokoyama, Appl. Phys. Express **10**, 102701 (2017).
6) H. Ishii, K. Otomo, J.-H. Hung, M. Tsutsumi, H. Yokoyama, and T. Nemoto, Biomed. Opt. Express. **10**, 3104 (2019).
7) K. Otomo, T. Hibi, Y.-C. Fang, J.-H. Hung, M. Tsutsumi, R. Kawakami, H. Yokoyama, and T. Nemoto, Biomed. Opt. Express **9**, 2671 (2018).
8) B. R. Rankin and S. W. Hell, Opt. Express **17**, 15679 (2009).
9) T. H. Runcorn, R. T. Murray, E. J. R. Kelleher, and J. R. Taylor, presented at Lasers Congress 2016 (ASSL, LSC, LAC), 2016, p. ATh1A.3.
10) T. H. Runcorn, F. G. Gorlitz, R. T. Murray, and E. J. R. Kelleher, IEEE J. Sel. Top. Quantum Electron. **24**, 1 (2018).
11) J.-H. Hung, H.-J. Yan, K. Sato, H. Yamada, L.-H. Peng, and H. Yokoyama, presented at CLEO Pacific Rim Conf. 2018, p. W3A.36.
12) B. Hein, K. I. Willig, and S. W. Hell, Proc. Natl Acad. Sci. USA **105**, 14271 (2008).
13) U. V. Nagerl and T. Bonhoeffer, J. Neurosci. **30**, 9341 (2010).
14) S.-K. Hwang, J.-M. Liu, and J. K. White, IEEE J. Sel. Top. Quantum Electron. **10**, 974 (2004).
15) M. Pochet, T. Locke, and N. G. Usechak, IEEE Photonics J. **4**, 1881 (2012).
16) Y. Kusama, Y. Tanushi, M. Yokoyama, R. Kawakami, T. Hibi, Y. Kozawa, T. Nemoto, S. Sato, and H. Yokoyama, Opt. Express **22**, 5746 (2014).